ADVANCED FUNCTIONAL MATERIALS
www.afm-journal.de

How Water Can Affect Keratin: Hydration-Driven Recovery of Bighorn Sheep (*Ovis Canadensis*) Horns

Wei Huang, Alireza Zaheri, Wen Yang, David Kisailus, Robert O. Ritchie, Horacio Espinosa, and Joanna McKittrick**

Keratin is one of the most common structural biopolymers exhibiting high strength, toughness, and low density. It is found in various tissues such as hairs, feathers, horns, and hooves with various functionalities. For instance, horn keratin absorbs a large amount of energy during intraspecific fights. Keratinized tissues are permanent tissues because of their basic composition consisting of dead keratinized cells that are not able to remodel or regrow once broken or damaged. The lack of a self-healing mechanism presents a problem for horns, as they are under continued high risk from mechanical damage. In the present work, it is shown for the first time that a combination of material architecture and a water-assisted recovery mechanism, in the horn of bighorn sheep, endows them with shape and mechanical property recoverability after being subjected to severe compressive loading. Moreover, the effect of hydration is unraveled, on the material molecular structure and mechanical behavior, by means of synchrotron wide angle X-ray diffraction, Fourier transform infrared spectroscopy, nanoindentation, and in situ and ex situ tensile tests. The recovery and remodeling mechanism is anisotropic and quite distinct to the self-healing of living tissue such as bones.

1. Introduction

Biological materials show remarkable mechanical efficiency through the use of numerous natural constituent materials in hierarchical structural designs to develop a variety of functionalities in response to the ecological constraints.[1] Keratin is one of the most abundant structural biopolymers existing in animal appendages from a 1D form in hair, 2D in pangolin scales to 3D in horns and hooves.[2] Keratin functions as a protective layer from the environment with hair and skin, as a natural dermal armor for scales, and for fighting or defensing purposes with horns. For the latter case, bovids use their horns as weapons in intraspecific fights to enable reproductive success.[3] Due to the fighting speed and their weight, the repeated collisions between two species are invariably forceful.[4] As a consequence, horns have to evolve to be strong enough to support the extreme fighting forces, tough enough to prevent fracture and to absorb large amounts of impact energy, and light enough to be carried.[3a,5] More importantly, horns must recover from the accumulation of damages after impacts, since they are permanent structures and cannot be remodeled or regrown.[5a,6]

Natural materials with energy absorption characteristic, such as wood and bamboo, have been widely studied for their sustainable designs.[7] These materials possess lightweight cellular structures with remarkable resistance to buckling and flexural forces. Reconfiguration of cells in the systems would assist the energy absorption process that arises through plastic buckling deformation of the cell walls in a relatively large strain range.[8] This has led investigators to manufacture numerous metallic and polymeric cellular structures to serve as energy absorption barriers for crashworthiness applications.[9] Although energy absorbing cellular structures have

Dr. W. Huang, Prof. J. McKittrick
Materials Science and Engineering Program
University of California San Diego
La Jolla, CA, USA
E-mail: jmckittrick@ucsd.edu

Dr. A. Zaheri, Prof. H. Espinosa
Theoretical and Applied Mechanics Program
Northwestern University
Evanston, IL, USA
E-mail: espinosa@northwestern.edu

Dr. W. Yang
Department of NanoEngineering
University of California
San Diego, La Jolla, CA, USA

The ORCID identification number(s) for the author(s) of this article can be found under https://doi.org/10.1002/adfm.201901077.

Prof. D. Kisailus
Department of Chemical and Environment Engineering
University of California
Riverside, CA, USA

Prof. R. O. Ritchie
Department of Materials Science and Engineering
University of California
Berkeley, CA, USA

Prof. H. Espinosa
Department of Mechanical Engineering
Northwestern University
Evanston, IL, USA

Prof. J. McKittrick
Department of Mechanical and Aerospace Engineering
University of California San Diego
La Jolla, CA, USA

DOI: 10.1002/adfm.201901077

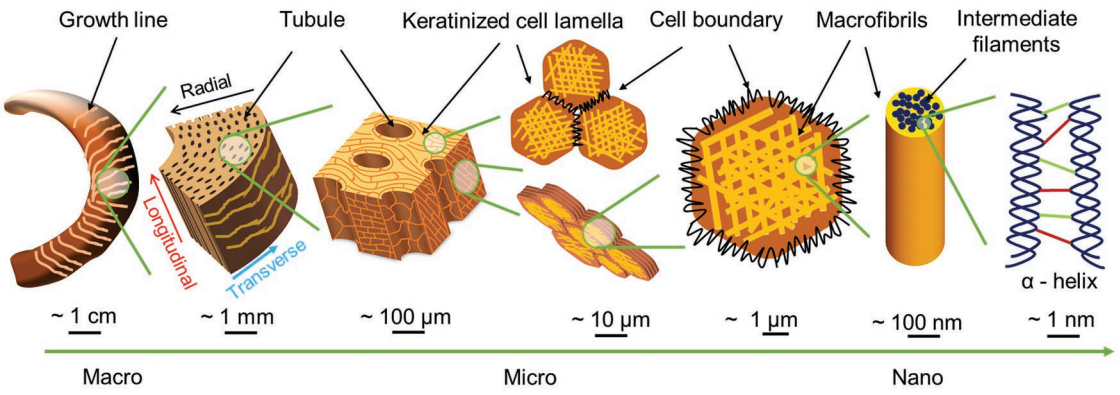

Figure 1. The hierarchical structure of the bighorn sheep horn. Adapted with permission.[11] Copyright 2017, Elsevier.

been widely used for impact resistance, analogous behavior has been reported in bighorn sheep horns conceived by the contribution of synergistic interactions between structural elements over different length-scales,[10] as described below.

The hierarchical structure of the horn is shown in **Figure 1**a.[11] At the microscale, hollow tubules with elliptical cross-sections (major axis ≈59 μm, minor axis ≈25 μm) were found extending from the base to the tip of the horn along the growth direction. Three directions can be defined: a longitudinal direction, which is in the growth direction, parallel with the tubules; a radial direction, which is the impact direction of the horn; and a transverse direction, which is orthogonal to the other two directions. Keratin cells (20–30 μm in diameter, 1–2 μm in thickness) are arranged in a layer-by-layer configuration, forming a lamellar structure surrounding the tubules. At the nanoscale, the cytoskeleton of the cells consists of macrofibrils with diameter ≈200 nm. The macrofibrils consist of bundles of aligned crystalline intermediate filaments (IFs) (≈7–10 nm in diameter) embedded in an amorphous matrix to create a polymer/polymer composite.[12] The macrofibrils are arranged randomly in the plane of the cells. At the molecular scale, the keratin polypeptide chains have a helical secondary protein structure, which is the α-helix. Two of the α-helix twist together and form coiled-coil dimers, which are the main components of the IFs.[13]

The mechanical properties and deformation mechanisms in natural materials result from the properties of a combination of structural elements over different length-scales and from environmental effects.[2a,14] In the case of keratinized materials, the properties in different orientations and their hydration sensitivity have been examined in previous studies.[15] For example, the arrangement of the keratin cells in pangolin scales was found to be an important factor determining their mechanical properties. The spatial distribution of the laminated cells was proposed to modulate the crack propagation direction, thereby affecting the fracture toughness.[2c] Approximately 40% higher compressive strength was observed in the direction perpendicular to the cell lamellae, while the compressive modulus was constant under different loading directions.[15b] In the case of horn, anisotropic behavior in the dry samples was observed, where energy absorption (area under the stress–strain curve) was highest in the impact direction (radial) than for the others.[11] This stemmed from the arrangement of the lamellae in different orientations, with the impact direction perpendicular to the cell lamellae. In the other two directions, parallel to the cell lamellae, buckling and shear banding of the lamellae under compressive loading was observed.[11] Full rehydration of horn samples resulted in more isotropic properties.[11] Moreover, fully hydrated samples showed a lower Young's modulus and energy absorption in both quasistatic and impact compression tests due to the increased mobility of polymer chains.[2b,10b,15a]

An interesting phenomenon elicited by hydration is the recoverability of shape and mechanical properties after deformation. This shape-memory feature is seen in hair from different species, and has been studies in terms of factors such as deformation, viscoelasticity, chemical groups, and water-assisted recovery.[16] It was found that heat (<100 °C) stabilizes the shape of deformed hair, while water stimulates the recovery of hair to its original shape.[16] It was speculated that both heat and water molecules could induce the reformation of breaks in the original hydrogen bonds (HBs) via a molecular recovery mechanism to create new HBs, to realize shape fixation and recovery.[16] HBs were proposed to be acting as switches, controlled by the water molecules to turn on the shape memory mechanism.[17] Microscopic damage caused by indentation of pangolin scales was recovered by hydration, which indicated that this dermal armor could recuperate from penetration injury caused by predators.[18] The shape memory effect present in cellular solid keratin material in peacock tail feathers was also studied.[19] After six cycles of 90% compression loading, both the compressive strength and energy absorption were retained by hydration recovery. The activation energy for relaxation was significantly decreased by hydration, which made this recovery behavior possible. The recovery of horn samples after compressive deformation and hydration was first introduced in our previous work.[11] Specifically, fully rehydrated horn samples were restored to their original dimensions after 30% deformation, in contrast to the dried specimens, in which microstructural damage and fracture were observed.[11]

Although the hierarchical structure and energy absorption properties at different strain rates of bighorn sheep horn have been investigated in previous studies,[11,15a] the recovery behavior of horns, especially involving the role of tubules, remains unclear. Hence, in this work we investigate the water assisted shape memory effect in bighorn sheep horn, which

could prove useful for future advances in the bioinspired designs of recoverable energy absorption structural materials. The present work focuses on two main outstanding issues: i) the understanding of the role of water in influencing the horn structure at the molecular level, and ii) the effects that this has on the mechanical behavior, specifically to discern the hydration-driven recovery properties and deformation mechanisms in horn keratin after severe compression along different orientations.

2. Results and Discussions

2.1. Water Effects on the Structure of Horn Keratin

Figure 2a shows a schematic diagram of X-rays passing through the transverse direction of a dry horn sample. The resulting diffraction pattern (Figure S3, Supporting Information) shows the periodicities of α-helix crystal structure that are indicated in the pattern, including a 0.5 nm arc in the longitudinal direction and a 1 nm arc in the radial direction; this is in agreement with the diffraction patterns of human hair and stratum corneum keratin.[20] This corresponded to the macrofibrils (yellow lines and dots) and IF arrangements, as shown in the schematic diagram in Figure 2a.

The periodic d-spacings in both the longitudinal (x) and radial (y) directions were deduced from the 2D diffraction patterns for both dry and fully rehydrated samples (Figure S3, Supporting Information). The peak intensities of the 0.5 and 1 nm d-spacings in dry and fully hydrated conditions are plotted in Figure 2b. Both intensities decreased after full hydration, which are likely a result of a decrease in the IF density in the matrix due to matrix swelling. It has been shown in wool and hair fibers that water acts as a plasticizer in the amorphous matrix while having no effect on the IFs.[21] This is corroborated with the current results, since the d-spacings of the α-helix in the hydrated samples remained the same. By using wide-angle X-ray diffraction (WAXD), for the first time we have verified that water molecules are absorbed by the amorphous matrix during hydration. By contrast, for matrix-free hagfish slime, Fudge and Gosline[22] found that the IFs absorbed water. Our results point out to the importance of the matrix in preferentially absorbing water and stabilizing the IFs.

Fourier transform infrared spectroscopy (FTIR) spectra from samples with the three different hydration states are shown in Figure 2c. Amide A&B, I, II, and III features were identified, according to the notation in previous studies.[23] The change in intensities and wavenumbers of the characteristic peaks of amide I, II, and III (orange, blue, and black dashed lines) indicated that water molecules had broken the HBs.[16,17] The wavenumbers of C=O stretching (amide I) and N−H bending (amide II) increased during hydration, indicating that new HBs formed between the amino acids and water molecules. It was found that the relative intensity of the N−H bonds compared to the C=O bonds decreased as the water content increased (green dashed lines in Figure 2c). This confirms that the water

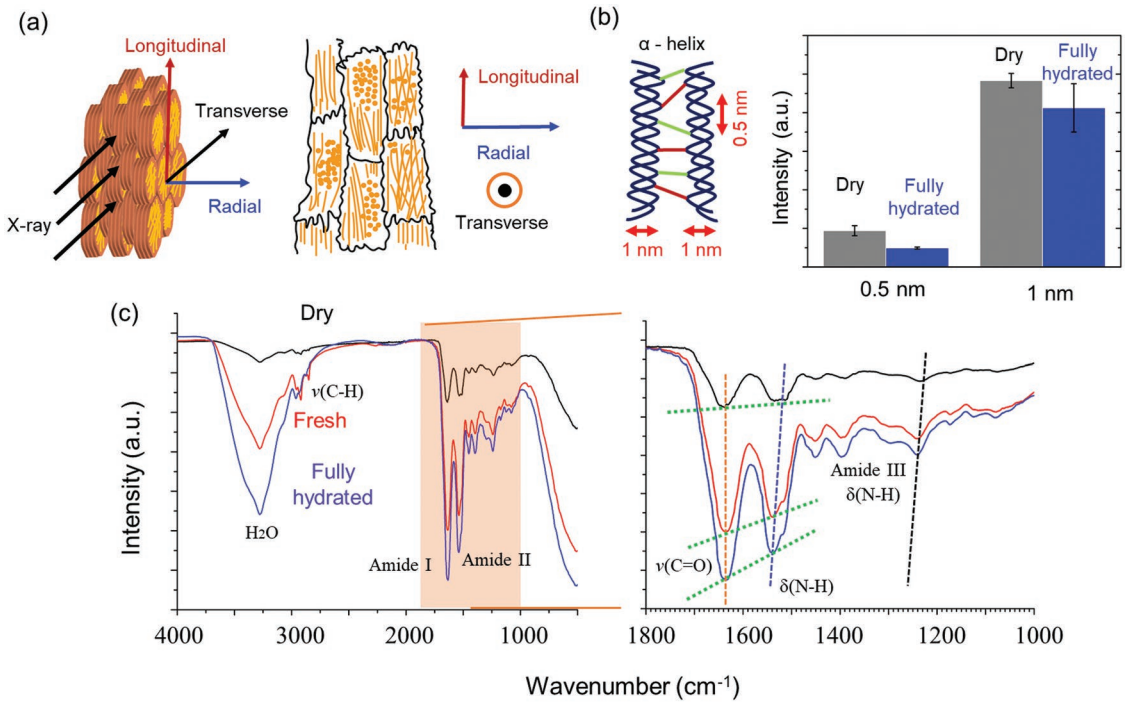

Figure 2. a) Schematic diagram of samples used for the synchrotron wide-angle X-ray diffraction (WAXD) experiments. The X-rays pass through transverse direction, parallel with the cell planes. Macrofibril (yellow lines and dots) orientation is shown in the accompanying schematic diagram. The IFs align in the same direction as the macrofibrils,[10a,b] the yellow lines and dots also indicate the orientation of IFs. b) Intensity of characteristic peaks at 0.5 and 1 nm in the WAXD diffraction pattern decrease after fully hydration. c) FTIR spectra of samples with different hydration states. Yellow, blue, and black dashed lines show the wavenumber shift of certain characteristic peaks. The green dashed line indicates the relative intensity ratio of C=O stretch and N−H bending peak changes for different hydration states.

molecules broke the HBs between the carbonyl group (C=O) and amino groups (N—H). New HBs formed due to the polar attraction between amino group (N—H) and H—O—H, which led to a decrease in the free N—H bonds, and finally a decrease in the N—H peak intensity in the hydrated samples. This result is important for the interpretation of the recovery process, as discussed below.

2.2. Water Effects on Tensile and Creep Properties

In situ tensile tests with WAXD of dry and fully hydrated samples in the longitudinal direction were conducted to measure the sample and IF failure strains (Figure S4, Supporting Information). The tensile stress as a function of the sample and IF strain is plotted in **Figure 3**a. The IF tensile strain was calculated from the d-spacing changes from the WAXD patterns (Figure S5, Supporting Information). Fully hydrated samples showed a larger failure strain (≈35%) than dry samples (≈5%), whereas dry samples have higher tensile strength and Young's modulus. The IF strain in the dry samples was <1%, which was attributed to brittle fracture of the sample. It has been well recognized that the amorphous matrix in dry keratin is stiff and rigid;[6,21b,24] this supports the majority of the tensile stress, thereby leading to a small failure strain in the IFs. In the fully hydrated samples, the IF failure strain (≈7%) was much higher than in the dry samples (Figure 3a). During hydration, FTIR and WAXD results demonstrated that water molecules diffused into the amorphous matrix phase and broke the HBs, which weakened the matrix. As a result, the IFs could be stretched to a larger deformation. However, the IF failure strain (≈7%) was only one fifth of the sample strain (≈35%), suggesting that the IFs pulled out from the matrix. It has been shown both experimentally and theoretically that the hydrogen bonding in α-helix and β-sheet of crystalline proteins could provide stiffness as well as energy dissipation strategies by breaking and reforming these weak bonds.[25] In the current study, we give evidence that in the presence of both α-helix crystalline and amorphous phases, hydrogen bonds are more easily broken in the amorphous matrix, leading to the decrease of stiffness in the matrix.

The stress–strain curves of the ex situ tensile tests on samples with different hydration states are shown in Figure 3b. The dry samples fractured after ≈5% strain but have the highest stiffness and tensile strength, consistent with the in situ WAXD results. The fresh samples fractured at ≈40% strain, higher than the other two conditions. Figure 3c–e shows schematic diagrams and scanning electron microscopy (SEM) images of the fracture surfaces. Brittle fracture occurred at 45° in the dry samples (Figure S4, Supporting Information) with the fractured lamellae as shown in Figure 3c. No fiber pull-out or breakage was observed, indicating matrix failure. For the fresh samples, the macrofibrils were pulled out from the matrix and fractured (Figure 3d). This suggests that the macrofibrils were able to carry some load before sample failure, leading to a large failure strain. It has been shown that both hair and wool fibers can sustain ≈50% tensile strain prior to fracture at both low (20% RH)

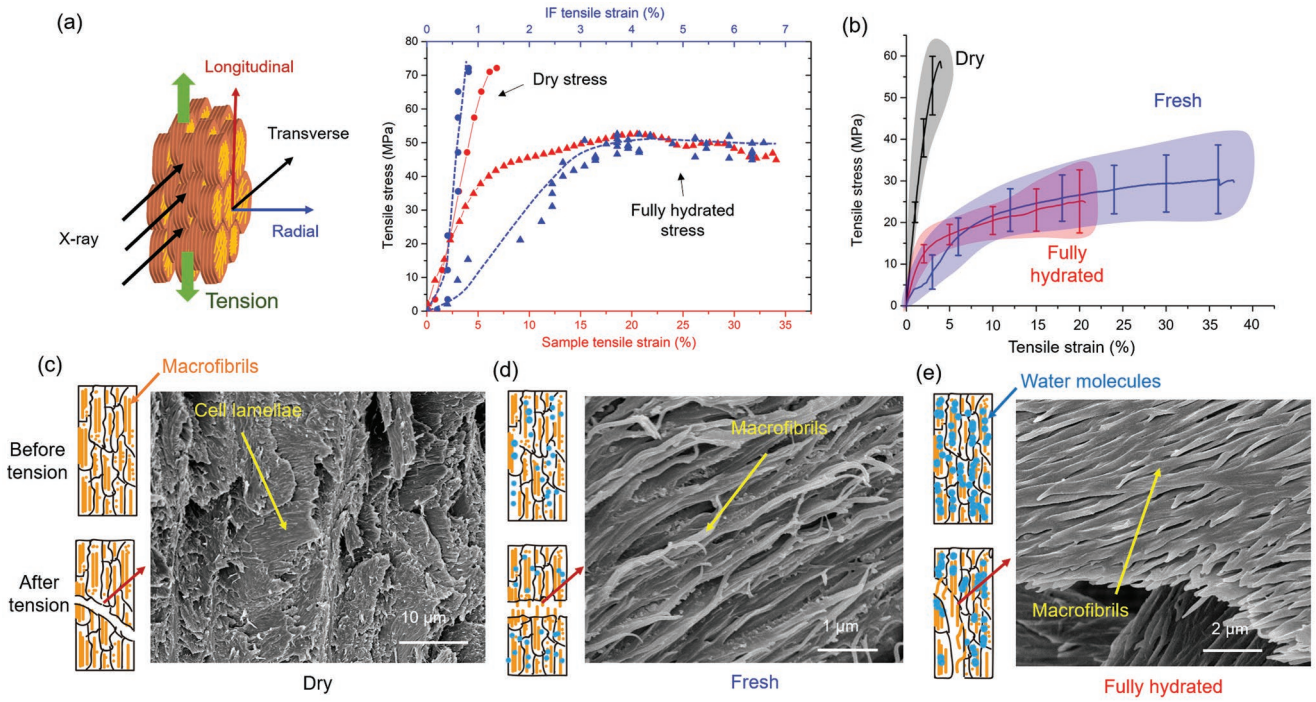

Figure 3. Water effects on the tensile behavior of horn samples. a) Schematic diagram of the test samples that were loaded in the longitudinal direction. Plots of tensile stress as a function of intermediate filament (IF) strain (blue) and sample tensile strain (red) in both dry (dots) and fully hydrated (triangles) conditions measured in in situ tensile tests are shown. b) Stress–strain curves from ex situ tensile tests for different hydration states. Dry samples show the highest tensile strength, while fresh samples had the highest tensile strain. c) Fracture surface of the dry samples showing brittle failure. Cell lamellae are shown (yellow arrow). d) Fracture surface of fresh samples. Macrofibrils pulled out and breakages are found. e) Fracture surface of sample in fully hydrated condition. Macrofibrils were pulled out from the matrix with no apparent breakage of fibers.

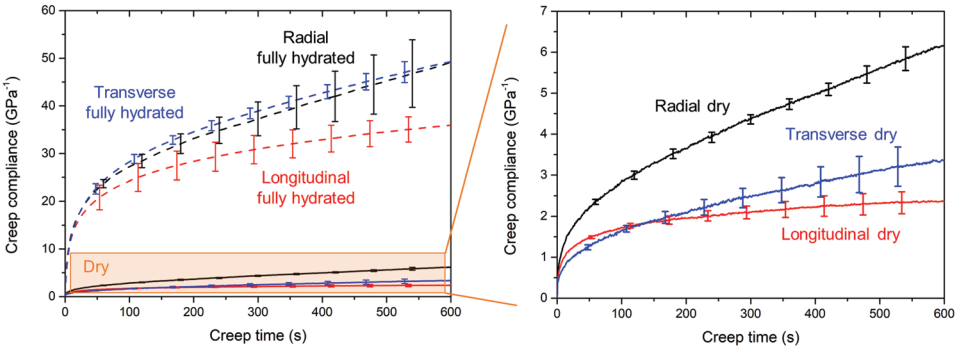

Figure 4. Creep compliance of horn samples, in the longitudinal, radial, and transverse directions, in dried and fully hydrated states, as a function of time, measured through flat punch nanoindentation.

and high (100% RH) relative humidity conditions.[15c,26] The fracture surface of a fully hydrated sample, shown in Figure 3e, indicates that the macrofibrils were directly pulled out from the matrix. This verifies the previous observations made for the in situ tests that the IFs are pulled-out from the matrix in the fully hydrated condition.

Water effects on the creep properties of horn samples were characterized by nanoindentation. Indentation load–displacement curves for the horn samples are provided in Figure S6 (Supporting Information). The variation of $J(t)$ for different orientation and hydration is shown in **Figure 4**. The curves for the fully hydrated samples reveal a large increase in creep compliance, $J(t)$, which results in higher strain due to viscous flow. This indicates that water molecules mediate the extensive network of secondary bonds, such as HBs between the amino and carboxyl groups in the amorphous keratin molecular chains, thereby increasing the mobility of the matrix molecules rather than increasing the cross-linking.[2b,27] In the dry samples, the differences in $J(t)$ came from the orientation of lamellae as well as IFs arrangements. The experimental data reveal that it is much easier to deform the sample in the direction perpendicular to the cell planes (radial direction) than in the directions parallel to the cell planes (longitudinal and transverse directions). However, for fully hydrated samples, the weakened amorphous matrix increases the creep deformation, leading to a more isotropic behavior.

2.3. Water Assisted Recoverable Behaviors

The stress–strain curves under different compression cycles up to 50% strain and for the different orientations are shown in **Figure 5**a–c. This maximum strain was selected based on previous observations that shear band formation and densification occurred at higher strains. The deformed samples were recovered in water at room temperature for 25 h. Higher temperatures (i.e., 70 °C) could accelerate the recovery process (≈20 h for recovery), however, not significantly. In the longitudinal (Figure 5a) and transverse (Figure 5b) directions, the samples fractured after three cycles. Within these three cycles, the stiffness and yield strength decreased slightly after the first cycle, in longitudinal direction, while no obvious change of the mechanical properties was found in transverse direction. In the radial direction (Figure 5c), the stiffness and yield strength, as well as the shape of the stress–strain curves remained constant in the first three cycles. Both stiffness and yield strength decreased ≈30% at the fourth cycle and then remained constant again, which presumably was the result of damage accumulation during the first three cycles. In terms of the energy absorption capability, ≈64% energy absorption amount remained after six cycles, indicating the durability of horns under cyclic deformation in the impact direction.

Optical microscopy images were taken before and after the first recovery. Figure 5d–f shows the sample surfaces after compression to 50% strain after the first cycle in different orientations. In the longitudinal direction, shear bands, delamination, and microfibril pull-out were observed (Figure 5d). In the transverse direction, more severe shear bands were observed, and cracks propagated from the vertices of adjacent tubules (Figure 5e). The orientation of the major axis of the cross-section of the elliptical tubule slightly changed (yellow dashed lines) due to the shear force applied along the major axis. In the radial direction (Figure 5f), no obvious cracks were found but only closure of the tubules. After recovery by hydration, corresponding optical microscopy (OM) images of the damaged surfaces were retaken as a comparison (Figure 5g–i). In both the longitudinal and transverse directions, the shear bands disappeared (Figure 5g,h), and the orientation of major axis of the tubules in the transverse direction returned to their original orientation (Figure 5h). However, delamination, cracks, and microfibril pull-out remained (Figure 5g). In the radial direction, the tubules reopened by hydration (Figure 5i). The recovery of the horn samples, however, has limitations: some of the damage modes can be recovered, such as reopening of the closed tubules, the unbuckling of tubules, and reorientation of the keratin cells, whereas others cannot, such as delamination, microfibril pull-out, and cracks between laminated cells. FTIR of samples after compression and recovery were conducted (Figure S8, Supporting Information), showing water molecules break the hydrogen bonds between C=O and N−H groups, highly abundant in proteins, during the recovery process, while after recovery and dehydration in air, the hydrogen bonds between these two groups reform.[23]

To gain a better understanding of the role of tubules played during compression and recovery tests, horn samples without tubules were identified in a region ≈15 mm beneath the impact

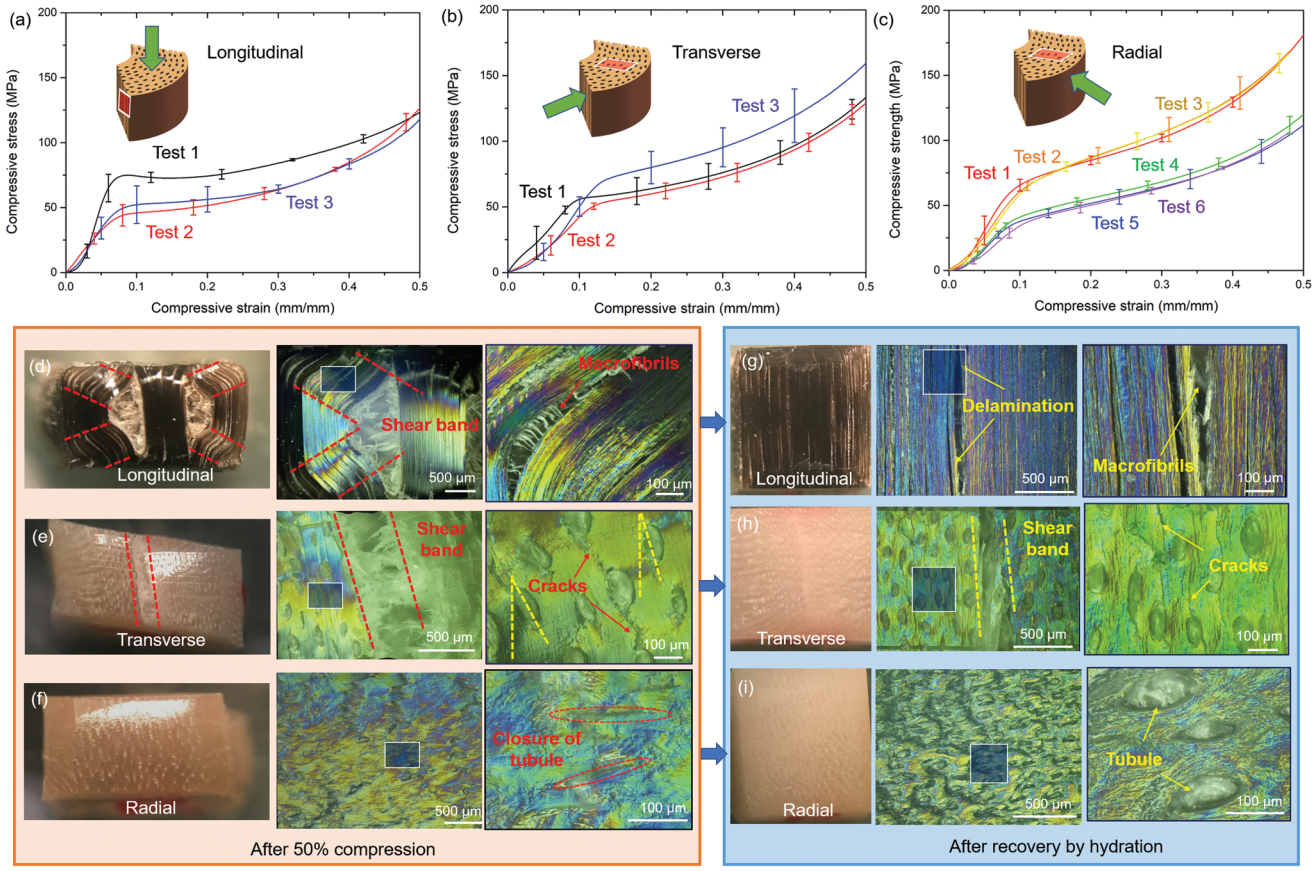

Figure 5. Recovery tests after 50% compressive deformation of samples in different loading orientations: a) Stress–strain curves in the longitudinal directions. Samples failed after Test 3. b) Stress–strain curves in the transverse direction. Samples failed after Test 3. c) Stress–strain curves of horn loading in the radial direction for different loading cycles. Stiffness and yield strength slightly decrease after the third cycle, then are constant from Tests 4 to 6. d) Photographs and microscopy images of the sample in the longitudinal direction. Shear bands and microfibril breakage are observed. e) Microscopy images of the sample in the transverse direction. Shear bands and cracks are observed. Yellow dashed lines show the axis of the major axis of ellipse changed direction after compression. f) Microscopy images of the sample in the radial direction. Closure of tubules is observed. Sample surface images after hydration for 24 h after compressive deformation. g) Longitudinal direction: Shear bands disappear but delamination and microfiber breakage remain. h) Transverse direction: Shear bands and cracks are not recovered. i) Radial direction: The tubules reopened after hydration.

surface of horn. Quasistatic compression tests in different orientations were performed and compared with the results of samples with tubules. **Figure 6**a,b shows that the stress–strain curves of both types of samples displayed a similar trend. The Young's modulus and yield strength are compared in Figure 6c. The Young's modulus in the radial direction, in the samples with tubules, was smaller than in samples without tubules, which is due to the stress concentration and closure of tubules. No significant differences were found in the Young's modulus along longitudinal and transverse directions between samples with and without tubules, which could be the reason that the stiffness in these two directions is limited by the buckling of cell lamellae, not plastic deformation of tubules. A higher yield strength in the longitudinal and transverse directions was found in the samples without tubules, indicating that for the samples with tubules, buckling and shearing of the tubules had occurred. The plateau stress was longer in samples without tubules in the longitudinal and transverse directions, implying that internal damage gradually occurred and thus maintained a constant stress level at a larger strain than in samples with tubules. Densification and stress increase were apparent at ≈60% strain in samples without tubules, while this occurred at a smaller (≈40–50%) strain in samples with tubules. These results indicate that tubules adjust the plateau stress and strain level in all the three directions. In terms of the amount of energy absorption at 70% compressive strain, samples with tubules had higher energy absorption than samples without tubules in all directions. However, samples without tubules may provide better protection for internal structures by controlling the stress at a constant level during large compression loadings while simultaneously absorbing significant amounts of energy.

The deformation mechanisms in samples without tubules were investigated to better identify features that contribute to energy absorption. Figure 6d shows samples in which the lamellae are observed. After compression in the radial direction, shear bands were present (Figure 6e), in contrast to samples with tubules (Figure 5f). After recovery, the cracks caused by shear bands were still present (Figure 6f). These results indicate that the tubules provide a path for stress redistribution,

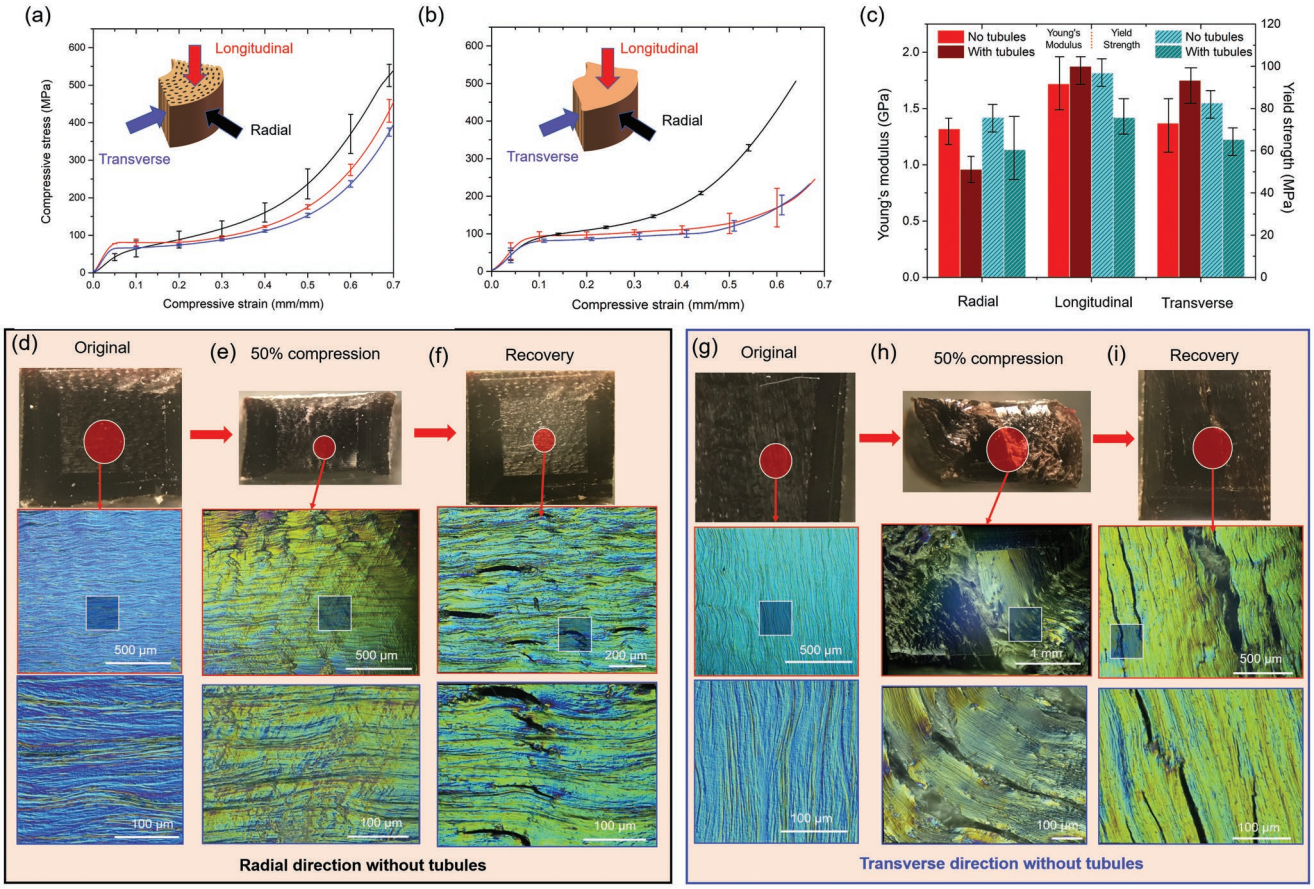

Figure 6. Quasistatic compression behavior of dry horn samples a) with and b) without tubules. c) Young's modulus and yield strength comparison between samples with and without tubules. d) Optical microscopy images of samples without tubules before compression in radial direction. e) Samples without tubules after 50% compression in the radial direction. X-shaped shear bands are shown on the surface. f) Samples without tubules recovered by hydration showing cracks and delamination. g) Samples without tubules prior to transverse compression. h) Samples in (g) after 50% compression. Large shear bands and cracks are observed on the surface. i) Samples in (h) after recovery by hydration. Large cracks and shear bands remain.

avoiding shear banding and cracking in the material during impact loading in the radial direction. For comparison, samples were also compressed in the transverse direction. Figure 6g shows the original structure without tubules before compression in the direction parallel to the lamellae. After 50% compression, severe shear banding, cracking, delamination, and fiber breakage are observed (Figure 6h). Although the overall shape was able to recover back after hydration, the damage, including cracks, delamination, and fiber breakage was not recovered (Figure 6i).

In summary, water-assisted recovery of structures after compression loading can only occur in samples with tubules and compressed in the radial direction. Interestingly, this is the active loading direction of bighorn sheep horns during intraspecific fighting. Indeed, it is known that "horning" exists in these Bovidae species, where the animals push their horns into wet mud or thrash them against vegetation.[5a] This can thus be considered as a rehydration process, which we verify in the current study can serve to promote recovery of any accumulated damage in the tissue caused by combat.

3. Conclusions

The effect of water on the nanostructure and mechanical properties of bighorn sheep horn samples were analyzed using synchrotron WAXD, SEM, optical microscopy, FTIR, and by in situ WAXD uniaxial tensile and ex situ compression and tensile tests for different orientations. The influence of tubules in the compression and hydration recovery behavior was specifically investigated by comparing samples with and without tubules found at different locations in the bighorn sheep horn. The main findings are:

- Hydration affects only the amorphous keratin matrix and does not modify the crystallinity of IFs. FTIR demonstrates that water molecules diffuse into the amorphous matrix and break the hydrogen bonds between carbonyl group (C=O) and amino groups (N−H), which lead to the recovery of deformed horn samples.
- In situ and ex situ tensile tests of horn samples under different hydration states (dry: ≈10 wt%, fresh: ≈15–20 wt%, wet: ≈30 wt%) show differences in IF strain and fracture behaviors

under tension. Dry samples had the highest strength but lowest tensile strain to failure due to brittle fracture: less than 1% strain is observed in the IFs in the dry samples. Fiber pull-out was observed in fully hydrated samples due to the plasticized matrix after water absorption; failure strains of ≈7% were now measured in the IFs in such fully hydrated samples. This was attributed to the weakened matrix, which allowed for a larger extent of deformation. Details and more quantitative characterization of how the hydrogen bonds will affect the mechanical properties of both crystalline and amorphous proteins as well as the combination of these two phases still needs further investigation.

- Nanoindentation experiments reveal that creep strains and compliance, along all orientations, are much higher under hydrated conditions. This is consistent with increased mobility of matrix protein molecules arising from hydration effects.
- The horn keratin structure can be recovered by hydration after severe compression (50% compressive strain). However, only samples in the radial direction can retain their mechanical properties after recovery, due to the absence of damage. By contrast, damage of the keratin cells during compression, in the longitudinal and transverse directions, remains. Recovery occurs after water molecules enter the amorphous matrix and interact with IFs through a process of breaking and reforming hydrogen bonds.
- The presence of tubules is critical to the recovery process. They act to redistribute the stress and thereby protect the keratin cells from damage under compression in the radial direction. X-shaped shear bands were found in samples without tubules, which cannot be recovered by hydration. However, samples with tubules show higher energy absorption capabilities in all three loading directions.

In conclusion, we have found that although horn keratins represent dead tissues that cannot regrow or remodel once damaged or fractured, they can still recover their shape and most of the mechanical properties under hydration. Analogous behavior has recently been found for tooth enamel.[28] Interestingly, in the horn keratins, the recovery mechanisms only occur in the impact (radial) direction due to the tubular structure. The present work thus shows that bighorn sheep horns are ideal materials evolved by nature to satisfy the mechanical requirements of repetitive compression and impacts. Moreover, the hydration-driven recovery mechanism of the tubular structure of the bighorn sheep horn keratin could provide inspiration for the design of new synthetic materials with superior shape-memory energy absorption properties.

4. Experimental Section

Acquisition and Preservation of Horn Samples: Two bighorn sheep (*Ovis canadensis*) horns were purchased from the Wilderness Trading Company (Pinedale, WY). The horns were then preserved at room temperature in dry condition for future use. The horns were estimated to be ≈6–8 years old with dimension ≈60 cm in length and ≈9 cm in diameter at the proximal region (Figure S1a, Supporting Information). It is unknown how long the horns had been stored in an ambient dry condition after harvesting, prior to our acquisition. The samples for our experiments were collected from the impact region, as shown in Figure S1a (Supporting Information). Apart from the dry samples, rehydrated samples were also prepared. Three dry samples were first weighed and then put in an oven (≈120 °C) for 24 h to fully dehydrate; these conditions were based on previous work on horn keratin.[10a] After measuring the weight, the samples were immersed in deionized (DI) water to acquire various water contents as a function of immersion time up to 300 min (Figure S2, Supporting Information). Due to the unavailability of fresh horns, samples with partial hydration were prepared to mimic the fresh state, on the basis that fresh horn has a water content of ≈15–20 wt%.[6,29]

Synchrotron WAXD: Synchrotron WAXD studies were conducted on the beamline 7.3.3 at the Advanced Light Source at Lawrence Berkeley National Laboratory (Berkeley, CA). Samples were cut with a diamond saw into thin films with thickness of ≈500 µm to improve the penetration of the X-rays. The samples were 10 mm in length (longitudinal direction) and 3 mm in width (radial direction). The sample dimensions were based on previous WAXD studies of biological materials.[30] Three samples were scanned before and after hydration. By aligning the transverse direction along the X-rays, the molecular structure in longitudinal and radial direction of the samples could be determined (Figure 2a). A 2D intensity map of the total scattering vector was acquired (q_x in longitudinal, q_y in radial). The diffraction patterns were further analyzed with data analysis software IGOR Pro (WaveMetrics, Inc., Lake Oswego, Oregon, USA). The corresponding real space length scale periodicity, the d-spacing ($d = 2\pi/q$), in the molecular structures was calculated. The d-spacing indicates the characteristic repeat and interatomic spacing in the α-helix molecular structure in the IFs.

In situ uniaxial tensile tests of dry and fully hydrated samples were also conducted with simultaneous real time WAXD measurements. The mechanical tests were performed with a custom-made rig using a 10 mm displacement stage and a 45 N load cell (Omega LC703-10, Norwalk, CT, USA). The tensile tests were performed at room temperature at a strain rate 10^{-3} s^{-1}. The sample was exposed to 10 keV X-rays for 0.5 s for ≈5 s intervals during the tensile testing to obtain the structural change through WAXD information during the tensile tests.

Attenuated Total Reflection-Fourier Transform Infrared Spectroscopy (ATR-FTIR): ATR-FTIR spectroscopy was conducted using a FTIR spectrophotometer (PerkinElmer, Waltham, MA, USA) to characterize the water effects on the chemical bonds of keratin. Nine samples with the same dimensions as for the WAXD tests were prepared. Scans were taken in the transverse direction. Three samples for each condition (dry, fresh, and fully hydrated) were characterized by ATR-FTIR and compared with previous results on hair.[15c,16,17]

Ex Situ Tensile Tests and Fracture Surface Imaging: Samples for uniaxial tensile testing were prepared with dimensions of 15 mm in length (longitudinal direction), 3 mm in width (radial direction), and 0.5 mm in thickness (transverse direction). Tensile loads were applied in the longitudinal direction using an Instron 3342 mechanical testing machine (Instron Corp., Norwood, MA) with a load cell of 500 N at a strain rate of 10^{-3} s^{-1}. At least five samples were tested in each condition (dry, fresh, and fully hydrated). The fracture surfaces were imaged with an ultrahigh resolution scanning electron microscope (SEM, FEI, Hillsboro, OR, USA). Before imaging, samples were fixed in 2.5% glutaraldehyde for 3 h and then dehydrated with an ethanol series (20%, 40%, 60%, 80%, 90%, 100% vol%). Samples were then placed in a critical point dryer (Auto Samdri 815A, Tousimis, Rockville, Maryland, USA). The tensile fracture surfaces were sputter coated with iridium using an Emitech K575X sputter coater (Quorum Technologies Ltd., UK) prior to SEM imaging.

Viscoelastic Behavior: Creep Tests: Understanding the effect of hydration on viscoelastic properties such as stress relaxation at the macroscale has been reported on the horn sheath.[29] However, viscoelastic properties have not been reported at a small scale. Here, the investigation of hydration effect on the viscoelastic behavior of horn samples was performed through nanoindentation. Indeed, nanoindentation techniques have been used in the past to study the creep behavior of bone[31] and synthetic polymeric materials.[32] In the present study on horn, creep tests and measurements of creep compliance at different orientations and hydration levels were conducted. Samples with

dimension 4 mm × 4 mm × 4 mm for each orientation were cut with a diamond saw, and smooth surfaces with a roughness not exceeding 20 nm were prepared with an ultramicrotome (Leica UC7/FC7 Cryo-Ultramicrotome, Buffalo Grove, IL, USA). The creep behavior of the dry samples was examined using a nanoindenter (MTS NanoIndenter XP, Eden Prairie, MN, USA) with a diamond flat-ended tip with a 10 µm diameter. At least three different locations were indented with a constant loading rate of 2.5 mN s^{-1} and 2 s loading time to avoid any viscous deformation. Subsequently, each indent was followed by 10 min hold time and unloaded at the same rate as the loading one. To test the creep behavior of the hydrated samples, the samples were immersed in DI water for three days, and they were kept hydrated throughout the indentation process by adding droplets of DI water. In order to correct for thermal drift effects, creep tests with the same procedure were conducted on fused silica. Using this data, thermal drift corrections were applied to the results obtained with horn samples. The samples were placed in the nanoindenter 48 h prior to the tests, to equilibrate to the ambient conditions.

The indentation creep compliance, $J(t)$, was measured based on a well-established method customary used for polymeric materials;[32b,33] namely, $J(t) = \varepsilon(t)/\sigma_0$. Here, σ_0 is the contact stress defined as the ratio of the constant indentation load over the contact area at the end of loading segment. $\varepsilon(t)$ is the indentation strain, which is measured as the ratio of displacement during holding at a constant load over the initial displacement at which the load first reaches maximum and becomes constant. Further details on the calculations of the creep compliance are given in Figures S6 and S7 in the Supporting Information.

Compression Recovery Tests: Compression samples (5 mm^3 cubes) were obtained from a region located ≈5 mm beneath the impact surface of the horn (Figure S1, Supporting Information). The sample surfaces were polished with an ultramicrotome (Leica EM UC6, Leica Microsystems Inc., Buffalo Grove, IL, USA) for OM imaging to characterize the microstructure after each cycle. The sample surfaces were imaged using a Keyence VHX 1000 OM (Keyence, Palatine, IL, USA) with differential interference contrast light to resolve the surface features. Samples were then compressed with a universal testing machine using a 30 kN load cell (Instron 3367 Dual Column Testing Systems, Instron, MA, USA) to 50% deformation, to avoid densification.[11] The recovery process was achieved by immersing the samples in DI water at room temperature for 25 h after compression, which returned the samples to the original dimensions. Samples were then kept at room temperature for three days to obtain a constant water content (≈10 wt%). Surfaces of the recovered samples were then imaged as a reference. Sample dimensions and weight were measured and compared with the original values before the next cycle of compression. The compression and recovery cycles were repeated until the samples were unable to return to their original dimensions.

Compression and recovery tests were also conducted to examine the role of the tubules. Regions ≈15 mm beneath the impact surface of the horn (Figure S1, Supporting Information) were found without tubules. Cubic samples (5 mm^3) in this area were prepared to perform compression and recovery tests to compare with the tubular samples. Compression and recovery tests were conducted in the three different directions. Since there are no tubules, the longitudinal and transverse directions were assumed identical. Images of the surfaces were only taken in the radial and transverse directions.

Supporting Information

Supporting Information is available from the Wiley Online Library or from the author.

Acknowledgements

The authors gratefully acknowledge financial support from a Multi-University Research Initiative through the Air Force Office of Scientific Research (Grant No. AFOSR-FA9550-15-1-0009) and a NSF Biomaterials Grant 1507978. The authors also acknowledge the use of beamline 7.3.3 at the Advanced Light Source at the Lawrence Berkeley National Laboratory, which is supported by the Office of Science, Office of Basic Energy Sciences, Division of Materials Sciences and Engineering of the US Department of Energy under Contract no. DE-AC02-05CH11231. The authors thank Mason Mackey at National Center for Microscopy and Imaging Research (NCMIR), Timo Meerloo and Ying Jones at Electron Microscopy Facility at UC San Diego for providing help with ultramicrotome. Additionally, the authors thank Ryan Anderson of the Nano3 Laboratory of CalIt2 for helping with the optical microscopy. This work was performed in part at the San Diego Nanotechnology Infrastructure (SDNI) of UCSD, a member of the National Nanotechnology Coordinated Infrastructure, which is supported by the National Science Foundation (Grant ECCS-1542148).

Conflict of Interest

The authors declare no conflict of interest.

Keywords

energy absorption, keratin, mechanical behavior, self-recovery, water effects

Received: February 3, 2019
Revised: April 8, 2019
Published online:

[1] a) M. A. Meyers, P. Y. Chen, A. Y. M. Lin, Y. Seki, *Prog. Mater. Sci.* **2008**, *53*, 1; b) U. G. K. Wegst, M. F. Ashby, *Philos. Mag.* **2004**, *84*, 2167; c) L. J. Gibson, M. F. Ashby, G. N. Karam, U. Wegst, H. R. Shercliff, *Proc. R. Soc. A* **1995**, *450*, 141.

[2] a) P. Y. Chen, J. McKittrick, M. A. Meyers, *Prog. Mater. Sci.* **2012**, *57*, 1492; b) B. Wang, W. Yang, J. McKittrick, M. A. Meyers, *Prog. Mater. Sci.* **2016**, *76*, 229; c) M. J. Chon, M. Daly, B. Wang, X. Xiao, A. Zaheri, M. A. Meyers, H. D. Espinosa, *J. Mech. Behav. Biomed. Mater.* **2017**, *76*, 30.

[3] a) A. Kitchener, *J. Zool.* **1988**, *214*, 1; b) A. Kitchener, *J. Zool.* **1985**, *205*, 191.

[4] a) M. Courtney, A. Courtney, *Sheep Collisions: the Good, the Bad, and the TBI*, *arXiv preprint arXiv:0711.3804* **2007**; b) A. Drake, T. L. H. Donahue, M. Stansloski, K. Fox, B. B. Wheatley, S. W. Donahue, *Acta Biomater.* **2016**, *44*, 41.

[5] a) A. Kitchener, *J. Zool.* **1987**, *213*, 621; b) Y. Zhang, W. Huang, C. Hayashi, J. Gatesy, J. McKittrick, *J. R. Soc., Interface* **2018**, *15*, 20180093.

[6] A. Kitchener, J. F. V. Vincent, *J. Mater. Sci.* **1987**, *22*, 1385.

[7] a) L. J. Gibson, M. F. Ashby, *Cellular Solids: Structure and Properties*, Cambridge University Press, Cambridge, UK **1999**; b) S. E. Naleway, M. M. Porter, J. McKittrick, M. A. Meyers, *Adv. Mater.* **2015**, *27*, 5455; c) U. G. K. Wegst, H. Bai, E. Saiz, A. P. Tomsia, R. O. Ritchie, *Nat. Mater.* **2015**, *14*, 23; d) J. McKittrick, P. Y. Chen, L. Tombolato, E. E. Novitskaya, M. W. Trim, G. A. Hirata, E. A. Olevsky, M. F. Horstemeyer, M. A. Meyers, *Mater. Sci. Eng., C* **2010**, *30*, 331; e) I. Maskery, N. Aboulkhair, A. Aremu, C. Tuck, I. Ashcroft, R. D. Wildman, R. J. Hague, *Mater. Sci. Eng., A* **2016**, *670*, 264.

[8] a) S. Maiti, L. Gibson, M. Ashby, *Acta Metall.* **1984**, *32*, 1963; b) L. J. Gibson, *Mater. Sci. Eng., A* **1989**, *110*, 1.

[9] a) M. Avalle, G. Belingardi, R. Montanini, *Int. J. Impact Eng.* **2001**, *25*, 455; b) L. Cui, S. Kiernan, M. D. Gilchrist, *Mater. Sci. Eng., A*

2009, *507*, 215; c) L. Di Landro, G. Sala, D. Olivieri, *Polym. Test.* **2002**, *21*, 217.
[10] a) L. Tombolato, E. E. Novitskaya, P. Y. Chen, F. A. Sheppard, J. McKittrick, *Acta Biomater.* **2010**, *6*, 319; b) M. W. Trim, M. F. Horstemeyer, H. Rhee, H. El Kadiri, L. N. Williams, J. Liao, K. B. Walters, J. McKittrick, S. J. Park, *Acta Biomater.* **2011**, *7*, 1228.
[11] W. Huang, A. Zaheri, J. Y. Jung, H. D. Espinosa, J. Mckittrick, *Acta Biomater.* **2017**, *64*, 1.
[12] a) M. Kadir, X. Wang, B. Zhu, J. Liu, D. Harland, C. Popescu, *J. Struct. Biol.* **2017**, *198*, 116; b) C. Popescu, H. Höcker, *Chem. Soc. Rev.* **2007**, *36*, 1282.
[13] a) R. Fraser, T. MacRae, *J. Mol. Biol.* **1961**, *3*, 640; b) R. Fraser, T. MacRae, A. Miller, *J. Mol. Biol.* **1964**, *10*, 147.
[14] M. A. Meyers, P.-Y. Chen, *Biological Materials Science: Biological Materials, Bioinspired Materials, and Biomaterials*, Cambridge University Press, Cambridge, UK **2014**.
[15] a) K. L. Johnson, M. W. Trim, D. K. Francis, W. R. Whittington, J. A. Miller, C. E. Bennett, M. F. Horstemeyer, *Acta Biomater.* **2017**, *48*, 300; b) B. Wang, W. Yang, V. R. Sherman, M. A. Meyers, *Acta Biomater.* **2016**, *41*, 60; c) Y. Yu, W. Yang, M. A. Meyers, *Acta Biomater.* **2017**, *64*, 15.
[16] X. Xiao, H. Zhou, K. Qian, *Smart Mater. Struct.* **2017**, *26*, 035023.
[17] X. Xiao, J. Hu, *Sci. Rep.* **2016**, *6*, 26393.
[18] Z. Liu, D. Jiao, Z. Weng, Z. Zhang, *J. Mech. Behav. Biomed. Mater.* **2016**, *56*, 14.
[19] Z. Liu, D. Jiao, Z. Zhang, *Biomaterials* **2015**, *65*, 13.
[20] a) F.-C. Yang, Y. Zhang, M. C. Rheinstädter, *PeerJ* **2014**, *2*, e619; b) Y. Zhang, R. J. Alsop, A. Soomro, F.-C. Yang, M. C. Rheinstädter, *PeerJ* **2015**, *3*, e1296; c) J.-C. Garson, J. Doucet, J.-L. Lévêque, G. Tsoucaris, *J. Invest. Dermatol.* **1991**, *96*, 43; d) M. E. Rafik, J. Doucet, F. Briki, *Biophys. J.* **2004**, *86*, 3893.
[21] a) F.-J. Wortmann, S. De Jong, *Text. Res. J.* **1985**, *55*, 750; b) M. Feughelman, *Mechanical Properties and Structure of Alpha-Keratin Fibres: Wool, Human Hair and Related Fibres*, UNSW Press, Sydney, Australia **1997**.
[22] D. S. Fudge, J. M. Gosline, *Proc. R. Soc. London, Ser. B* **2004**, *271*, 291.
[23] a) P. Garidel, H. Schott, *BioProcess Int.* **2006**, *4*, 48; b) A. Barth, *Biochim. Biophys. Acta* **2007**, *1767*, 1073; c) J. M. Cardamone, *J. Mol. Struct.* **2010**, *969*, 97.
[24] M. Feughelman, M. Robinson, *Text. Res. J.* **1971**, *41*, 469.
[25] a) T. Ackbarow, X. Chen, S. Keten, M. J. Buehler, *Proc. Natl. Acad. Sci. USA* **2007**, *104*, 16410; b) S. Keten, Z. Xu, B. Ihle, M. J. Buehler, *Nat. Mater.* **2010**, *9*, 359; c) Z. Qin, M. J. Buehler, L. Kreplak, *J. Biomech.* **2010**, *43*, 15.
[26] C. E. Reese, H. Eyring, *Text. Res. J.* **1950**, *20*, 743.
[27] J. Bertram, J. Gosline, *J. Exp. Biol.* **1987**, *130*, 121.
[28] Z. Liu, Z. Weng, Z.-F. Zhai, N. Huang, Z.-J. Zhang, J. Tan, C. Jiang, D. Jiao, G. Tan, J. Zhang, *Acta Biomater.* **2018**, *81*, 267.
[29] A. Kitchener, *J. Mater. Sci. Lett.* **1987**, *6*, 321.
[30] a) W. Yang, V. R. Sherman, B. Gludovatz, E. Schaible, P. Stewart, R. O. Ritchie, M. A. Meyers, *Nat. Commun.* **2015**, *6*, 6649; b) E. A. Zimmermann, B. Gludovatz, E. Schaible, N. K. Dave, W. Yang, M. A. Meyers, R. O. Ritchie, *Nat. Commun.* **2013**, *4*, 2634.
[31] a) Z. Wu, T. A. Baker, T. C. Ovaert, G. L. Niebur, *J. Biomech.* **2011**, *44*, 1066; b) N. Rodriguez-Florez, M. L. Oyen, S. J. Shefelbine, *J. Mech. Behav. Biomed. Mater.* **2013**, *18*, 90.
[32] a) H. Lu, B. Wang, J. Ma, G. Huang, H. Viswanathan, *Mech. Time-Depend. Mater.* **2003**, *7*, 189; b) E. Herbert, W. Oliver, A. Lumsdaine, G. M. Pharr, *J. Mater. Res.* **2009**, *24*, 626.
[33] S. Yang, Y.-W. Zhang, K. Zeng, *J. Appl. Phys.* **2004**, *95*, 3655.